Fire Safety Journal 44 (2009) 1095–1102

Contents lists available at ScienceDirect

Fire Safety Journal

journal homepage: www.elsevier.com/locate/firesaf

Experimental validation of a numerical model for the transport of firebrands

S. Kortas [a,b], P. Mindykowski [a], J.L. Consalvi [a,*], H. Mhiri [b], B. Porterie [a]

[a] Université de Provence, IUSTI/UMR CNRS 6595, 5 rue E. Fermi, 13453 Marseille Cedex 13, France
[b] Unité de Thermique et Thermodynamique des Procédés Industriels, Ecole Nationale d'Ingénieurs de Monastir, Avenue Ibn El Jazzar, 5019 Monastir, Tunisia

ARTICLE INFO

Article history:
Received 14 January 2009
Received in revised form
29 July 2009
Accepted 5 August 2009
Available online 12 September 2009

Keywords:
Firebrands
Cylinder
Disk-shaped
Transport
Modelling
Validation

ABSTRACT

The paper deals with the experimental validation of a numerical model for the transport and combustion of cylindrical and disk-shaped firebrands. The model solves the conservation equations of brand mass, kinetic and angular momentum, and volume. Validation consists in predicting the mass and spatial distributions of glowing firebrands that were produced from the experimental generator developed by Manzello and coworkers [S.L. Manzello, J.R. Shields, T.G. Cleary, A. Maranghides, W.E. Mell, J.C. Yang, Y. Hayashi, D. Nii, T. Kurita, On the development and characterization of a firebrand generator, Fire Saf. J. 43 (2008) 258–268]. Ten thousand firebrands per run are released with initial conditions that are randomly generated according to probability distribution functions deduced from experimental mass and spatial distributions under no-wind conditions. Whatever the wind conditions considered, numerical results are found to be in good agreement with experimental data.

1. Introduction

Spotting refers to the ignition of either forest fuel beds or houses ahead of the main fire by firebrands produced by burning vegetation. The spotting process can be divided into three stages: (i) the generation of firebrands, (ii) their subsequent transport by the plume and the prevailing wind, and (iii) the ignition of the receptive fuel. A limited number of studies have been conducted on the determination of the size and mass distributions of firebrands generated from burning trees [1–3] and on the ignition of fuel beds by firebrands [3–8]. On the other hand, since the capability of brands to ignite new spot fires depends primarily on their energetic content at landing, the modeling of the trajectories and burning rates of flying embers has received a considerable amount of attention in the past [9–24].

Full scale validation of a model for the transport and combustion of firebrands is a difficult task, so most of the comparisons between models and experiments remain qualitative. The aim of the present study is to validate a transport model on a large scale by comparison with experimental data reported by Manzello et al. [1] using a firebrand generator.

2. Model

2.1. Firebrand motion

In this study cylindrical and disk-shaped firebrands are considered. Fig. 1 shows the schematic of a firebrand, the corresponding coordinate systems and the notations. In agreement with the experiments of Manzello et al. [1] firebrands are assumed to be released into a horizontal wind in such a way that their trajectory lies in the xz plane. $\mathbf{x} = [x,y,z]$ is the inertial coordinate system. $\mathbf{x}' = [x',y,z']$ is the particle coordinate system with its origin being at the particle mass center and its axes being the principal axes. $\mathbf{x}'' = [x'',y,z'']$ is the co-moving coordinate system with its origin coinciding with that of the particle frame and its axes being parallel to the axes of the inertial frame. Firebrand trajectories are subjected to drag, lift, and gravitational forces, and also to pitching moments due to the non-coincidence of the centers of mass and hydrodynamic forces (see Fig. 1).

Using these assumptions the horizontal and vertical projection of the momentum equation and the conservation of the angular momentum become

$$m_f \frac{du_{fx}}{dt} = \frac{1}{2}\rho_{film} A_p |\mathbf{u}_{rel}| (C_D u_{rel\,x} - C_L u_{rel\,z}) \quad (1)$$

$$m_f \frac{du_{fz}}{dt} = \frac{1}{2}\rho_{film} A_p |\mathbf{u}_{rel}| (C_D u_{relz} + C_L u_{relx}) - m_f g \quad (2)$$

* Corresponding author. Tel.: +33 491 106 927; fax: +33 491 106 969.
E-mail address: Jean-Louis.Consalvi@polytech.univ-mrs.fr (J.L. Consalvi).

0379-7112/$ - see front matter © 2009 Elsevier Ltd. All rights reserved.
doi:10.1016/j.firesaf.2009.08.001

Nomenclature

A_p projected area (m^2)
C_D drag coefficient
C_L lift coefficient
C_M pitching moment coefficient
D_{eff} firebrand effective diameter
D_f firebrand diameter (m)
d horizontal distance measured from the generator (m)
$E = \tau_{f0}/D_f$ aspect ratio
$\mathbf{F}_D$ drag force ($kg\,m/s^2$)
$\mathbf{F}_G$ gravitational force ($kg\,m/s^2$)
$\mathbf{F}_L$ lift force ($kg\,m/s^2$)
g gravity acceleration (m/s^2)
I_f moment inertia ($kg\,m^2$)
$\mathbf{M}$ pitching moment ($kg/m^2/s^2$)
m_f mass of the firebrand (kg)
p, pdf probability distribution function
Pr Prandtl number
R random number
$Re = \rho_{film} D_f |\mathbf{u}_{rel}|/\mu_{film}$ Reynolds number
U_{wind} wind velocity (m/s)
$\mathbf{u}_f = [u_{fx},0,u_{fz}]$ firebrand velocity in the inertial frame (m/s)
$\mathbf{u}_g = [U_{wind},0,0]$ gas velocity (m/s)
$\mathbf{u}_{rel} = [u_{relx},0,u_{relz}]$ relative velocity (m/s)
$\mathbf{x} = [x,y,z]$ inertial coordinate system
$\mathbf{x}' = [x',y,z']$ particle coordinate system
$\mathbf{x}'' = [x'',y,z'']$ co-moving coordinate system
x_{cp} distance between the pressure-centre and the mass-centre of the particle

Greek letters

α incidence angle between $\mathbf{u}_{rel}$ and particle major axis (z') (rad)
β parameter of the Weibull distribution
κ parameter of the Weibull distribution
λ parameter of the Weibull distribution
μ viscosity (kg/m/s)
θ rotation angle (rad)
ρ density (kg/m^3)
τ_{f0} cylinder length or disk thickness (m)
ω_f firebrand spin (rad/s)

Subscripts

f firebrand
g gas
0 initial value, reference values

$$I_f \frac{d\omega_f}{dt} = \frac{1}{2}\rho_{film} C_M A_p D_f |\mathbf{u}_{rel}|^2 \tag{3}$$

The subscript *film* indicates that the associated gas property is taken at ambient pressure and at film temperature, which is defined as the arithmetic mean of the particle surface and ambient temperatures. The relative velocity is given by

$$\mathbf{u}_{rel} = \mathbf{u}_g - \mathbf{u}_f \tag{4}$$

The position and orientation of the firebrand are then obtained by integrating the following equations:

$$\frac{dx_f}{dt} = u_{fx} \tag{5}$$

$$\frac{dz_f}{dt} = u_{fz} \tag{6}$$

$$\frac{d\theta}{dt} = \omega_f \tag{7}$$

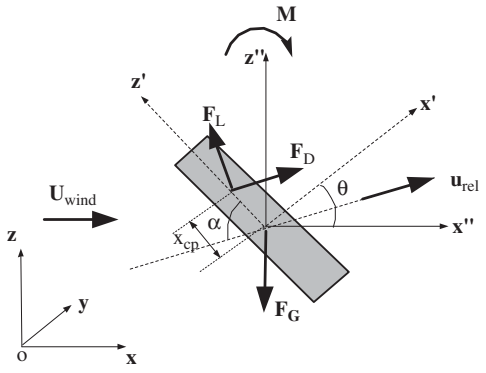

Fig. 1. Firebrand motion: notations and coordinate systems.

2.1.1. Cylinder aerodynamics

Cylinders are assumed to be transported with their axis (z') perpendicular to the relative velocity ($\alpha = \pi/2$ in Fig. 1) [21]. This assumption is expected to be valid for Reynolds numbers up to $O(10^4)$ [21] which is consistent with those encountered in this study. It implies that the induced lift force reduces to zero ($C_L = 0$ in Eqs. (1) and (2)). Moreover, the rotation of the particle (Eqs. (3) and (7)) is not considered since the incidence angle is prescribed.

The relationship for cylinder drag is taken from [21] and is expected to be accurate over a wide range of the Reynolds number ($10^{-4} < Re < 2\times10^5$):

$$C_D = 1.18 + \frac{6.8}{Re^{0.89}} + \frac{1.96}{Re^{0.5}} - \frac{4\times10^{-4} Re}{1 + 3.64\times10^{-7} Re^2} \tag{8}$$

2.1.2. Disk aerodynamics

Drag and lift coefficients are functions of the normal coefficient, C_N, and of the attack angle, α:

$$C_D = C_N \sin\alpha$$
$$C_L = C_N \cos\alpha + C_{Lr} \tag{9}$$

The normal coefficient is related to the drag coefficient for an attack angle of 90° by the following relationship [25]:

$$C_N = C_{D90} \frac{\sin\alpha}{0.56 + 0.44\sin\alpha} \tag{10}$$

According to Clift and Gauvin [26], C_{D90} can be expressed as a function of the particle Reynolds number:

$$C_{D90} = \frac{64}{\pi Re}(1 + 0.138\, Re^{0.792}), \quad Re \le 130$$
$$C_{D90} = 1.17, \quad Re > 130 \tag{11}$$

C_{Lr} accounts for Magnus effect due to the angular rotation velocities on the lift force. The following bilinear function is assumed for the component of lift coefficient induced by Magnus

effect [27]:

$$\begin{aligned} C_{Lr} &= 0.42(2.5\omega_f/\omega_{f0}) && \text{for } \omega_f/\omega_{f0} < 0.2 \\ C_{Lr} &= 0.42(0.375 + 0.625\omega_f/\omega_{f0}) && \text{for } \omega_f/\omega_{f0} \geq 0.2 \end{aligned} \quad (12)$$

where the steady-state angular velocity is $\omega_{f0} = 0.64U_{wind}/D_f$.

The moment of inertia is given by

$$I_f = \frac{m_f}{8}\left(\frac{D_f^2}{2} + \frac{2\tau_{f0}^2}{3}\right) \quad (13)$$

The pitching moment coefficient, C_M, is related to the normal force coefficient, C_N, and to the center of pressure position, x_{cp}, as

$$C_M = C_N x_{cp}/D_f \quad (14)$$

Holmes et al. [27] developed a segmented model of x_{cp}/D_f as a function of the angle of attack, which provides the best fit of the available experimental data,

$$\frac{x_{cp}}{D_f} = \begin{cases} 0.3 - 0.22(\alpha/38), & \alpha \leq 38^\circ \\ 0.08\cos[2(\alpha - 38)], & 38^\circ < \alpha < 82.5^\circ \\ 0, & 82.5^\circ \leq \alpha < 97.5^\circ \\ -0.08\cos[2(142 - \alpha)], & 97.5^\circ < \alpha \leq 142^\circ \\ -0.3 + 0.22[(180 - \alpha)/38], & 142^\circ < \alpha \leq 180^\circ \end{cases} \quad (15)$$

2.2. Firebrand combustion model

The firebrand combustion model that is used in this study is adopted from the works of Tse and Fernandez-Pello [20] and Anthenien et al. [21]. It yielded results in excellent agreement with the experimental data of Tarifa et al. [9,10] for the mass and surface loss of spherical, cylindrical, and disk-shaped firebrands. Since in this model brands are assumed to burn heterogeneously, their burning rate is enhanced at a high Reynolds number, without extinction due to flame blow-off. The model depends on a "quiescent atmosphere" burning constant β_0 which, for a given wood species, was found independent of both particle shape and Reynolds number. As recommended by Anthenien et al. [21] and Tse and Fernandez-Pello [20], the quiescent atmosphere burning constant β_0 is taken as being equal to $1.8 \times 10^{-7}\,m^2/s$, and the burning firebrand temperature to 993 K.

2.2.1. Burning cylinders

The model uses two equations to describe the changes in mass and volume during combustion; a "d-squared law" for the effective mass diameter and a "d-quarted law" for the size regression of the particle [21].

The effective mass diameter, D_{eff}, decreases as

$$\frac{dD_{eff}^2}{dt} = -\beta_0(1 + 0.276\,Re^{1/2}Pr^{1/3}) \quad (16)$$

where the Frössling relation is used to take into account the increase in burning rate due to a relative velocity between particle and air. The mass of the particle is then given by

$$m_f = \frac{\rho_f \pi D_{eff}^2 \tau_{f0}}{4} \quad (17)$$

and the evolution of the particle diameter, D_f, can be expressed as

$$\frac{dD_f^4}{dt} = -\frac{2\sqrt{3}}{E}[\beta_0(1 + 0.276\,Re^{1/2}\,Pr^{1/3})]^2 t \quad (18)$$

2.2.2. Burning disks

Disks are assumed to smoulder from the edge inward rather than over the entire face [21]. As a consequence, the disk thickness, τ_{f0} remains constant and the reaction to be diffusion controlled. The mass loss rate is expressed by

$$\frac{dm_f}{dt} = -\frac{\pi\rho_f\tau_{f0}}{4}\beta_0(1 + 0.276\,Re^{1/2}\,Pr^{1/3}) \quad (19)$$

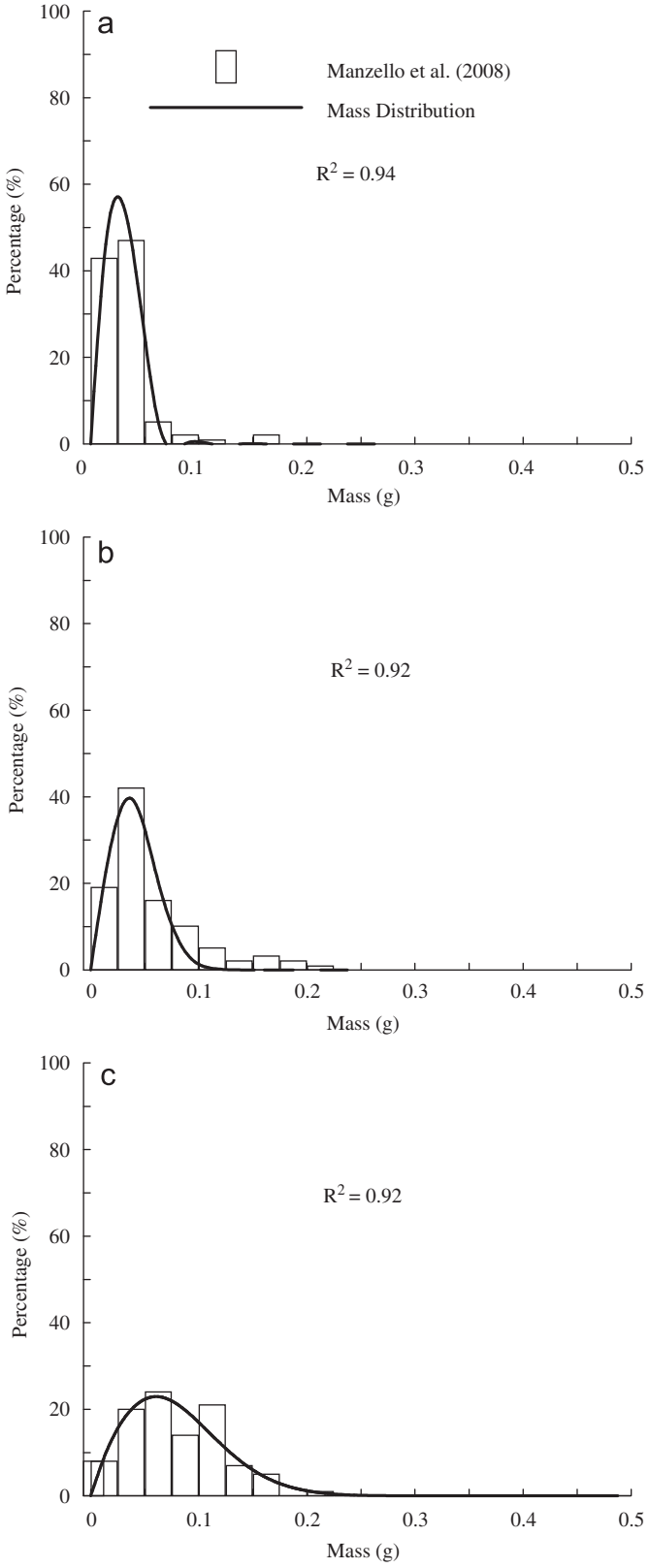

Fig. 2. Experimental (bars) and best fit (line) mass distributions under no-wind conditions: (a) cylinders of Type I, (b) cylinders of Type II, and (c) disks.

Following Anthenien et al. [21] we assume that the char is so fragile that it is broken off and disappears as soon as it is created, and therefore it does not affect the brand trajectory.

2.3. Numerical procedure

Differential equations are integrated by using a Euler scheme with a time step of 10^{-4} s. For cylinders, during a time step, the sequence of operations is the following: (i) determine the horizontal and vertical velocities by integrating Eqs. (1) and (2); (ii) determine the horizontal and vertical distances travelled by the firebrands by integrating Eqs. (5) and (6); (iii) determine the mass of the firebrand from Eqs. (16) and (17); and (iv) determine the firebrand diameter by integrating Eq. (18).

For disk-shaped firebrands, the sequence of operations is as follows: (i) determine the horizontal and vertical velocities and the angular velocities by integrating Eqs. (1)–(3); (ii) determine the horizontal and vertical distances travelled by the firebrands and the rotation angle by integrating Eqs. (5)–(7); (iii) determine the mass of the firebrand by integrating Eq. (19); and (iv) determine the diameter from the computed mass by considering that the thickness remains invariant.

3. Results and discussions

3.1. Description of the firebrand generator

Manzello et al. [1] constructed an experimental apparatus to generate a controlled and repeatable size and mass distribution of glowing firebrands. The generator was composed of a blower connected to a vertical duct in which a given mass of firebrands was deposited. Firebrands were released through a horizontal circular duct with a diameter of 15 cm located at a height of 2.175 m. In the experiments, 700 g of cylindrical or disk-shaped pieces of Ponderosa Pine wood with well determined properties were deposited into the firebrand generator. The pieces of wood were ignited by two propane burners for a total time of 45 s. After 45 s of ignition, the fan speed of the blower was increased to provide a 2 m/s flow inside the vertical duct in order to generate a continuous flux of glowing firebrands. The firebrand generator was installed inside a wind tunnel in order to influence the motion of the firebrands once released from the generator. Experiments were performed over a range of wind speeds from 0 to 9 m/s. A series of water pans was placed downstream of the generator in order to determine the size and mass distributions of the firebrands generated.

The simulation of the ignition and motion processes of firebrands inside the generator is beyond the scope of the present work. For comparison purposes, initial firebrand conditions at the generator exit (velocity, mass, and size) are determined from the experimental baseline (no wind) distributions.

Table 1
Fitting parameters of the baseline mass and spatial distributions.

Firebrand geometry	β	κ	λ
Mass distribution			
Cylinders of Type I	2.28×10^{-3} kg	2.21	3.27×10^{-5} kg
Cylinders of Type II	2.08×10^{-3} kg	2.12	4.65×10^{-5} kg
Disks	3×10^{-3} kg	1.89	9×10^{-4} kg
Spatial distribution			
Cylinders of Type I	48.17 m	2.51	1.07 m
Cylinders of Type II	48.23 m	2.69	1.09 m
Disks	48 m	2.57	1.99 m

3.2. Initial firebrand conditions

Two different kinds of cylindrical firebrands were deposited into the generator [1]. The first type, denoted hereafter as Type I,

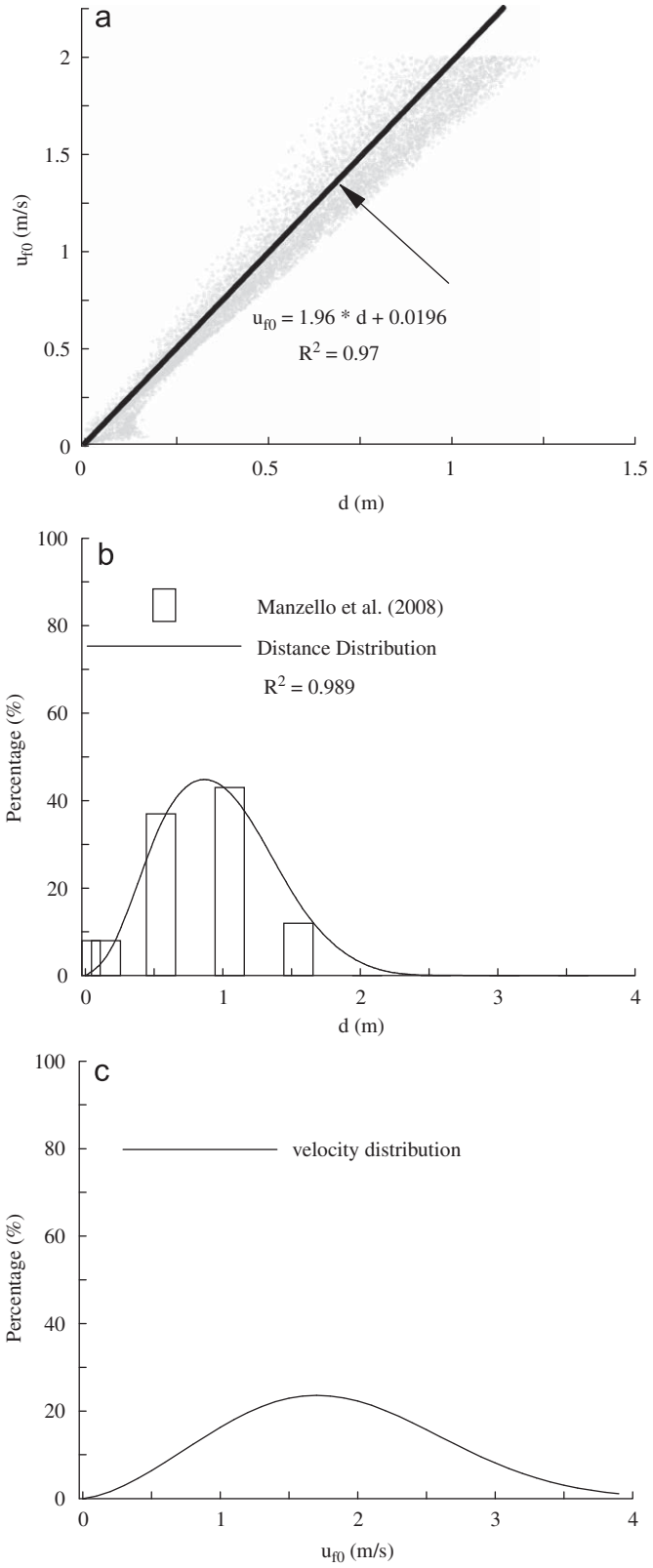

Fig. 3. Illustration in the case of disk-shaped firebrands of the procedure applied to determine the initial velocity distribution: (a) initial velocity as a function of the landing distance, (b) experimental (bars) and best fit (line) spatial distributions under no-wind conditions, and (c) initial velocity pdf.

had a diameter of 8 mm and a length of 50 mm. The second type, denoted hereafter as Type II, had a diameter of 12.5 mm and a length of 50 mm. In absence of wind, firebrands of Type I reach the ground with an average length of 13.5 mm (varying from $\tau_{f0,min}=6.5$ to $\tau_{f0,max}=20.5$ mm) and a diameter of 5.6 mm (varying from $D_{f0,min}=4.8$ to $D_{f0,max}=6.4$ mm) whereas those of Type II land with an average length of 12.2 mm (varying from $\tau_{f0,min}=6.4$ to $\tau_{f0,max}=18$ mm) and a diameter of 7.2 mm (varying from $D_{f0,min}=5.4$ to $D_{f0,max}=9$ mm).

Disk-shaped firebrands 6 mm in thickness and 25 mm in diameter were also deposited into the generator. Manzello et al. [1] observed that most disks broke up and reached the ground with a half-disk shape, the percentage of firebrands that reached the ground as disks being only 8% of the total mass. In absence of wind, they found that fallen disk-shaped firebrands had an average thickness of 5 mm (varying from $\tau_{f0,min}=4$ to $\tau_{f0,max}=6$ mm) and a diameter of 16 mm (varying from $D_{f0,min}=14$ to $D_{f0,max}=18$ mm). For the half-disk shapes, the average thickness was 5 mm (varying from $\tau_{f0,min}=3$ to $\tau_{f0,max}=7$ mm) and 14 mm in diameter (varying from $D_{f0,min}=10$ to $D_{f0,max}=18$ mm).

Table 2
Relationship between the initial velocity and the landing distance: values of the coefficients of the linear regression ($u_{f0}=ad+b$).

Firebrand geometry	a (s^{-1})	b (m/s)
Cylinders of Type I	2.31	10.7×10^{-2}
Cylinders of Type II	2.10	9.30×10^{-2}
Disks	1.96	1.96×10^{-2}

In the absence of wind the flying time of the firebrand was relatively short with respect to the time of combustion, so that firebrand properties (i.e. thickness or length, diameter and density) at landing did not differ significantly from those at the generator exit. As a consequence, the pdfs for initial firebrand properties at the generator exit can be approximated from the experimental baseline distributions at landing. This is why, for the present study, the initial diameter of firebrands is assumed to follow a uniform distribution:

$$p_D(D_{f0})=\begin{cases}\dfrac{1}{D_{f0,\max}-D_{f0,\min}} & \text{for } D_{f0,min}<D_{f0}<D_{f0,max}\\ 0 & \text{otherwise}\end{cases} \tag{20}$$

and similarly, for the initial firebrand length (cylinders) or thickness (disks),

$$p_\tau(\tau_{f0})=\begin{cases}\dfrac{1}{\tau_{f0,\max}-\tau_{f0,\min}} & \text{for } \tau_{f0,min}<\tau_{f0}<\tau_{f0,max}\\ 0 & \text{otherwise}\end{cases} \tag{21}$$

As shown in Fig. 2, the remaining mass at landing can be reasonably approximated by a Weibull distribution in the following form:

$$p_{m_f}(m_f)=\beta_m\left(\frac{\kappa_m}{\lambda_m}\right)\left(\frac{m_f}{\lambda_m}\right)^{\kappa_m-1}\exp\left[-\left(\frac{m_f}{\lambda_m}\right)^{\kappa_m}\right] \tag{22}$$

The parameters of the Weibull distributions are summarized in Table 1.

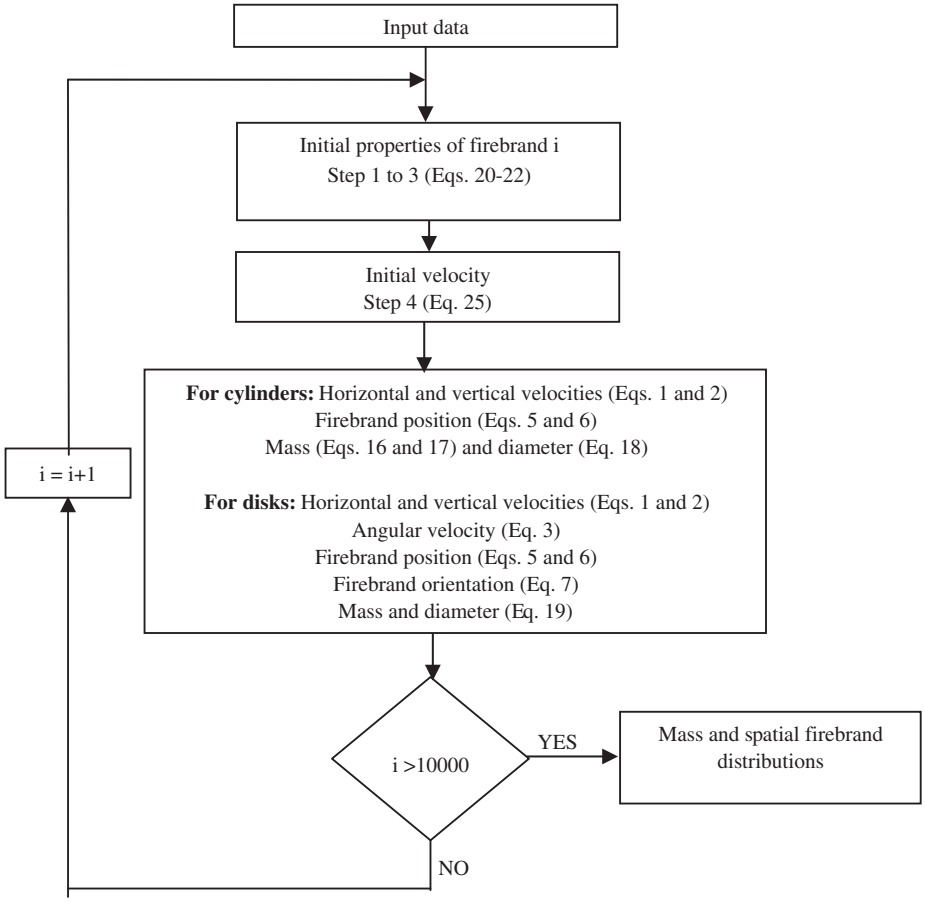

Fig. 4. Flow chart of the overall calculation process for cylindrical and disk-shaped firebrands.

The sequence of operations required to determine the initial properties of a firebrand at the generator exit can be described as follows:

1. For disk-shaped firebrands, generate a random number, R, between 0 and 1 to determine whether the brand generated is a disk or a half disk. If $R<\varphi$ the firebrand is a disk whereas it is a half disk if $R>\varphi$, where φ is a number adjusted so as to provide a percentage of disks of about 8% of the total mass, as observed experimentally.
2. Generate D_{f0} and τ_{f0} according to the pdfs given by Eqs. (20) and (21). Half-disk firebrands are assumed to have a disk shape with an equivalent diameter.
3. Generate the mass of the firebrand according to the pdf given by Eq. (22) in order to determine the firebrand density.

In order to simplify the problem we assume that the generator exit is a point source located at a height of 2.175 m and that the initial firebrand velocity is horizontal. The initial firebrand velocity distribution at the generator exit is determined from the experimental baseline distribution. The relationship between the landing distance and the initial velocity is obtained by releasing a series of 10^4 firebrands with initial velocities, u_{f0}, uniformly distributed in the range 0–2 m/s. For each firebrand geometry the relationship, $u_{f0}=\Phi(d)$, is found to be linear ($u_{f0}=ad+b$). This is illustrated in Fig. 3a for disk-shaped firebrands. The values of the coefficients a and b are given in Table 2. The pdf of the initial velocity is therefore determined from the experimental baseline spatial distribution, by using the following formula:

$$p_u(u_{f0})=p_d[\Phi^{-1}(u_{f0})]\frac{d\Phi^{-1}(u_{f0})}{du_{f0}} \tag{23}$$

Moreover, since the experimental distribution can be approximated by a Weibull function (see Fig. 3b for disks) as

$$p_d(d)=\beta_d\left(\frac{\kappa_d}{\lambda_d}\right)\left(\frac{d}{\lambda_d}\right)^{\kappa_d-1}\exp\left[-\left(\frac{d}{\lambda_d}\right)^{\kappa_d}\right] \tag{24}$$

Eq. (22) thus becomes

$$p_u(u_{f0})=\beta_d\left(\frac{\kappa_d}{a\lambda_d}\right)\left(\frac{u_{f0}-b}{a\lambda_d}\right)^{\kappa_d-1}\exp\left[-\left(\frac{u_{f0}-b}{a\lambda_d}\right)^{\kappa_d}\right] \tag{25}$$

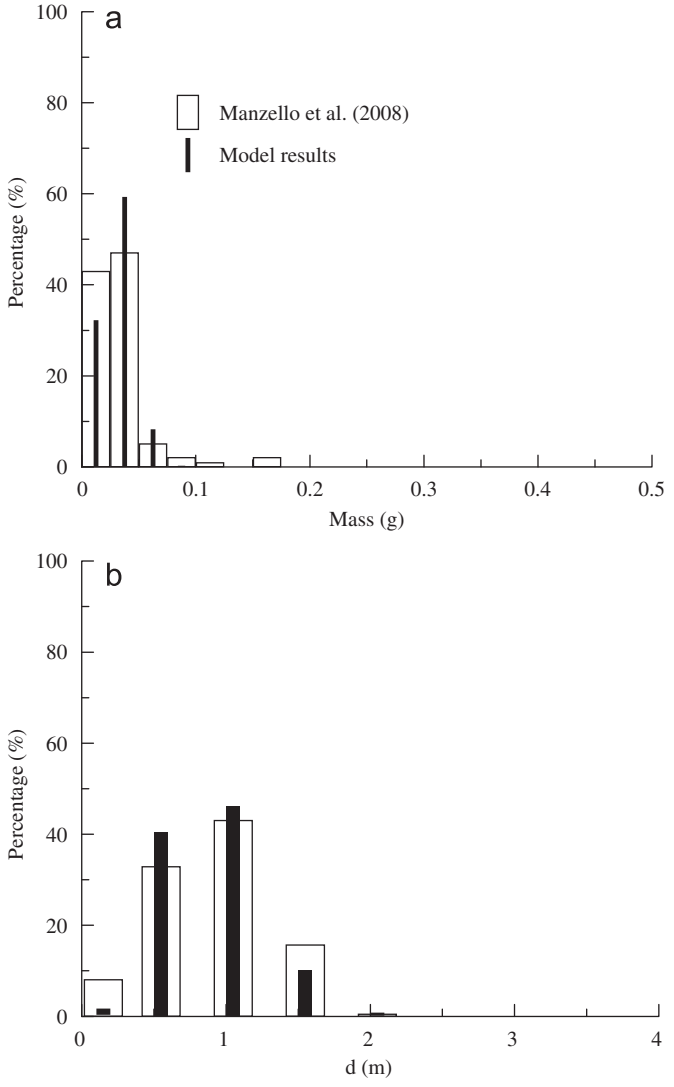

Fig. 5. Experiments vs. simulations under no-wind conditions: (a) mass and (b) spatial distributions for cylinders of Type I.

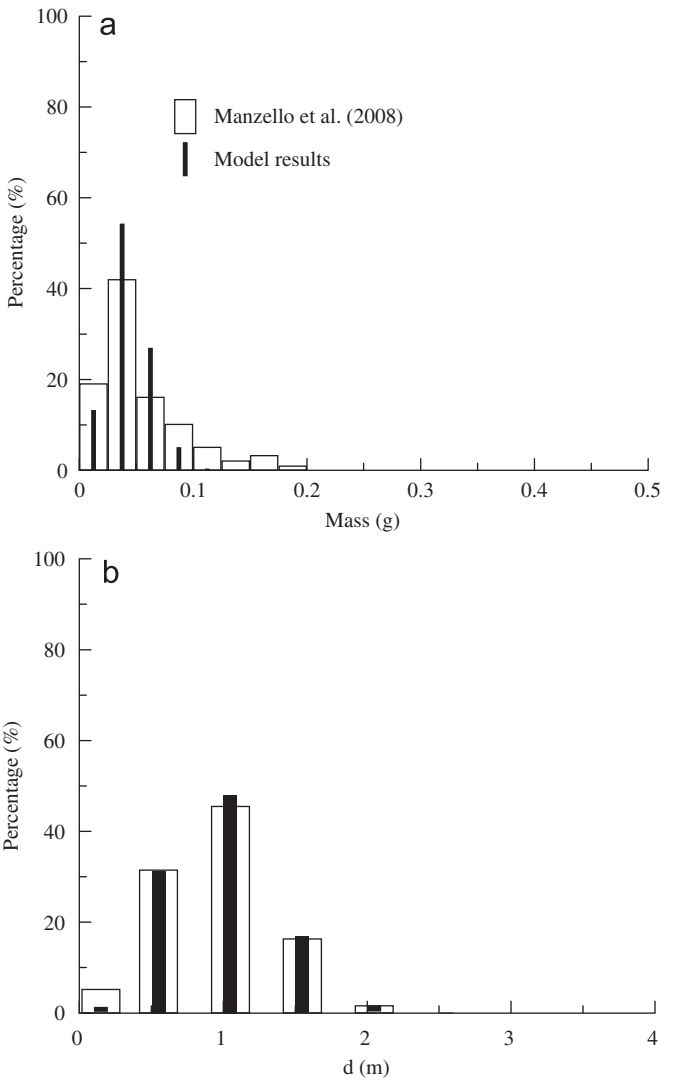

Fig. 6. Experiments vs. simulations under no-wind conditions: (a) mass and (b) spatial distributions for cylinder of Type II.

The probability density function of the initial velocity is also a Weibull function. It is shown in Fig. 3c for disks. For each firebrand geometry, β_d, κ_d, and λ_d are given in Table 1.

For each firebrand generated, a fourth step is added to the above sequence of operations. It consists in generating the initial velocity of the firebrand according to the pdf given by Eq. (25). For each run, ten thousand firebrands are released from the generator (see the calculation flow chart given in Fig. 4).

The relevance of the previously-determined pdf is assessed by performing a direct simulation in the absence of wind. As shown in Figs. 5–7 the experimental mass and spatial distributions are well reproduced by the model.

3.3. Wind effects

Wind effects are assumed to have no influence on the pdfs for initial velocity and brand properties at the generator exit. Fig. 8a and b show the landing distances for cylinders of Type I and II released into a wind of 9 m/s. In both cases, the simulations reproduced well the experimental data. For disk-shaped firebrands, landing distances as well as the spread of the distribution increase with wind speed (Fig. 9). The highest percentages of fallen firebrands are found in the range 1.8–2.3, 3.3–3.8, and 5.8–6.3 m for wind speeds of 3, 6, and 9 m/s respectively. Whatever the wind speed considered a good agreement between experimental and simulated spatial distributions is observed (Fig. 9).

4. Conclusions

A transport model for burning cylindrical and disk-shaped firebrands was used which consists in solving conservation equations for mass, volume, momentum, and angular momentum. Mass and spatial distributions under different wind conditions, obtained experimentally by Manzello et al. [1] using a generator of firebrands, were simulated by the release of a large amount of firebrands. The initial sizes, density, and velocity of each firebrand were randomly generated according to pdfs deduced from the experimental mass and spatial distributions in the absence of wind. Using these initial conditions, numerical simulations give results in good agreement with experimental data, whatever the wind speed considered.

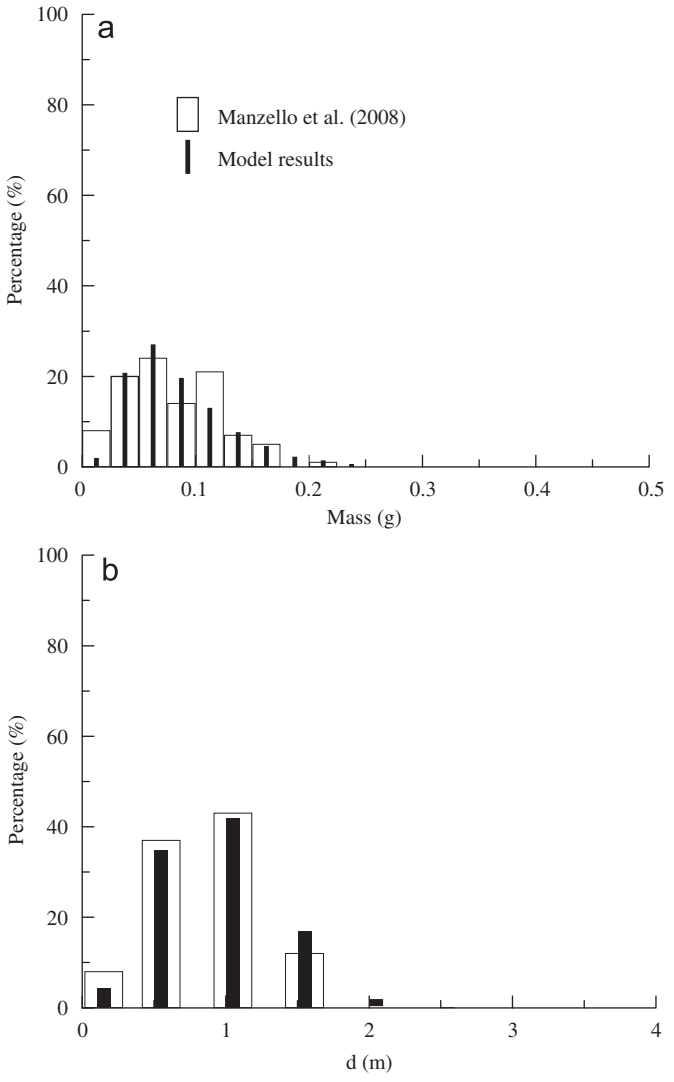

Fig. 7. Experiments vs. simulations under no-wind conditions: (a) mass and (b) spatial distributions for disk-shaped firebrands.

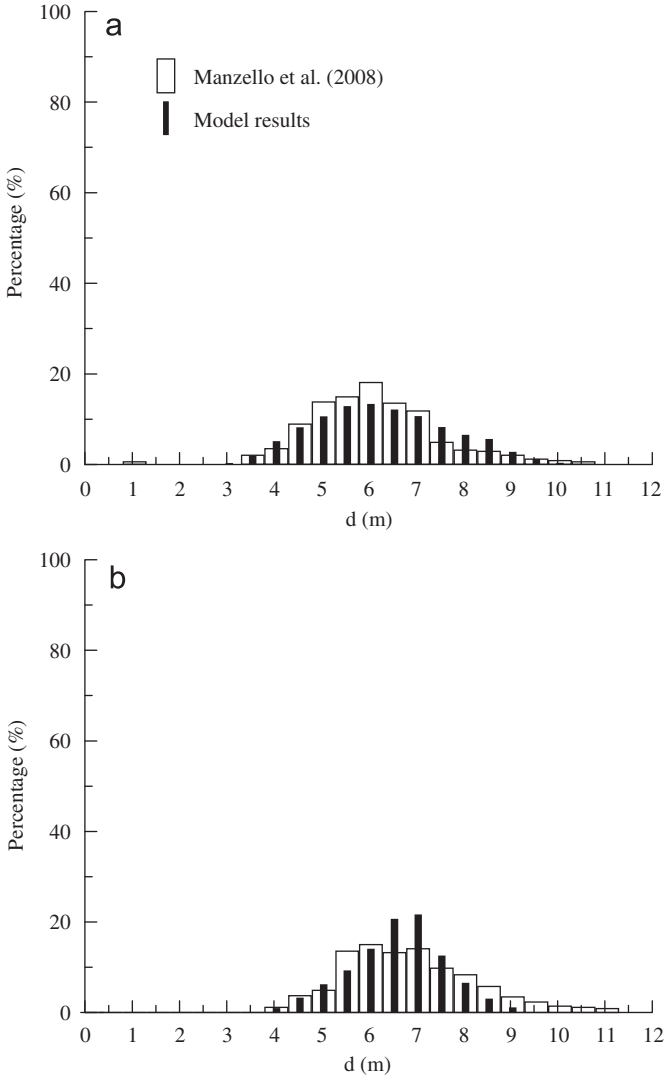

Fig. 8. Experiments vs. simulations for a wind speed of 9 m/s: (a) cylinders of Type I and (b) cylinders of Type II.

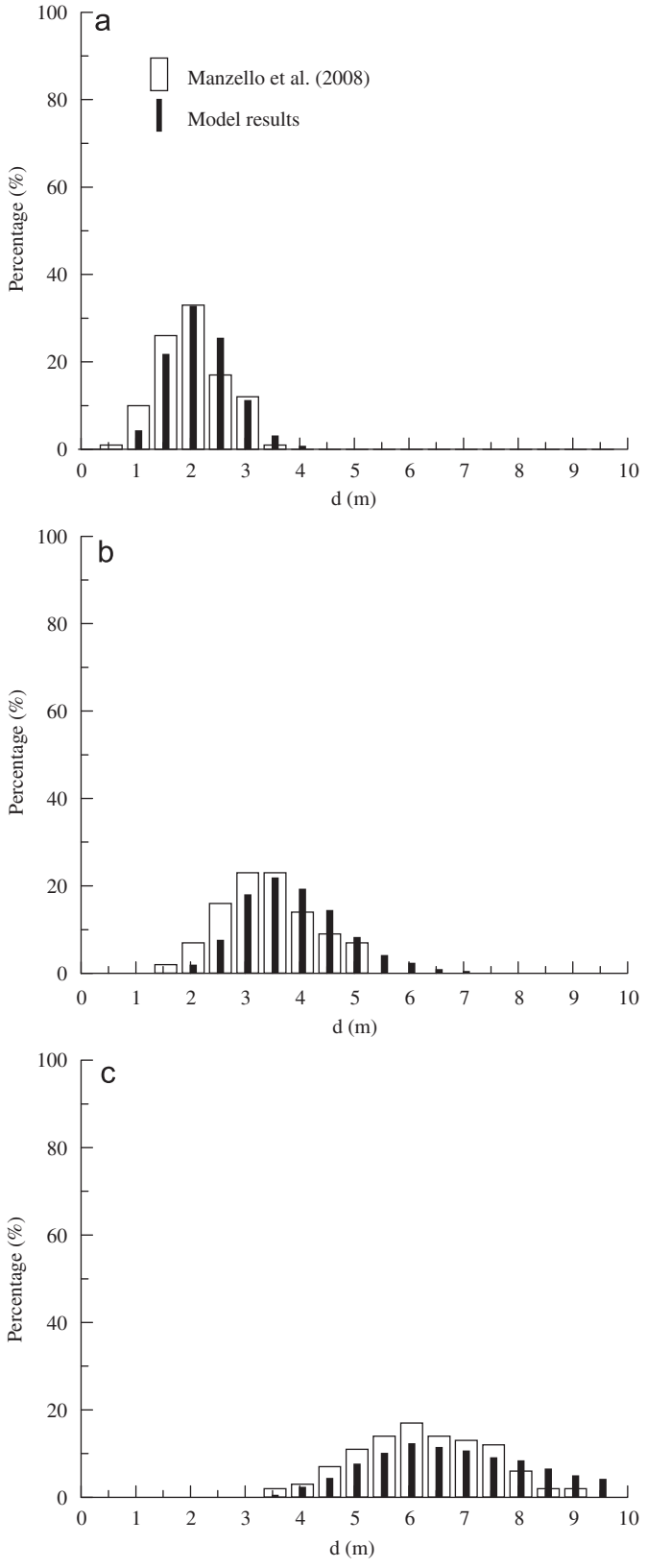

Fig. 9. Experiments vs. simulations for different wind speeds for disk-shaped firebrands. (a) 3 m/s, (b) 6 m/s, and (c) 9 m/s.

References

[1] S.L. Manzello, J.R. Shields, T.G. Cleary, A. Maranghides, W.E. Mell, J.C. Yang, Y. Hayashi, D. Nii, T. Kurita, On the development and characterization of a firebrand generator, Fire Saf. J. 43 (2008) 258–268.

[2] S.L. Manzello, A. Maranghides, W.E. Mell, Firebrand generation from burning vegetation, Int. J. Wildland Fire 16 (2007) 458–462.

[3] S.L. Manzello, T.G. Cleary, J.R. Shields, A. Maranghides, W.E. Mell, J.C. Yang, Experimental investigation of firebrands: generation and ignition of fuel beds, Fire Saf. J. 43 (2008) 226–233.

[4] A.M. Grishin, A.A. Dolgov, V.P. Zima, D.A. Kruychkov, V.V. Reino, A.N. Subbotin, R.S. Tsvyk, Ignition of a layer of combustible forest materials, Combust. Explos. Shock Waves 34 (1997) 613–620.

[5] A.I. Zvyagils'kaya, A.N. Subbotin, Influence of moisture content and heat and mass exchange with the surrounding medium on the critical conditions of initiation of surface fire, Combust. Explos. Shock Waves 32 (1996) 558–564.

[6] P.F. Ellis, Spotting and firebrand behaviour in dry eucalypt forest and the implications for fuel management in relation to fire suppression and to ember (firebrand) attack on houses, in: Proceedings of the Third International Wildland Fire Conference, Sidney, 2003.

[7] S.L. Manzello, T.G. Cleary, J.R. Shields, J.C. Yang, On the ignition of fuel beds by firebrands, Fire Mater. 30 (2006) 77–87.

[8] S.L. Manzello, T.G. Cleary, J.R. Shields, J.C. Yan, Ignition of mulch and grasses by firebrands in wildland–urban interface (WUI) fires, Int. J. Wildland Fire 15 (2006) 427–431.

[9] C.S. Tarifa, P.P. Del Notario, F.G. Moreno, On the flight paths and lifetimes of burning particles of wood, in: Tenth Symposium (International) on Combustion, The Combustion Institute, 1965, pp. 1021–1037.

[10] C.S. Tarifa, P.P. Del Notario, F.G. Moreno, A.R. Villa, Transport and combustion of firebrands, Final Report of Grants FG-SP-11 and FG-SP-146, US Department of Agriculture Forest Service, 1967.

[11] A. Muraszew, J.B. Fedele, W.C. Kuby, Trajectory of firebrands in and out of fire whirls, Combust. Flame 30 (1970) 321–324.

[12] F.A. Albini, Spot fire distance from burning trees—a predictive model, General Technical Report INT-56, USDA Forest Service, 1979.

[13] F.A. Albini, Spot fire distance from isolated sources—extensions of a predictive model, General Technical Report INT-309, USDA Forest Service, 1981.

[14] F.A. Albini, Potential spotting distance from wind-driven surfaces fires, Research Paper INT-309, USDA Forest Service, 1983.

[15] F.A. Albini, Transport of firebrands by line thermals, Combust. Sci. Technol. 32 (1983) 277–288.

[16] J.P. Woycheese, P.J. Pagni, D. Liepman, Brand lofting above large-scale fires, in: Proceedings of the Second International Conference on Fire Research and Engineering, Boston, USA, 1998.

[17] J.P. Woycheese, P.J. Pagni, Combustion models for wooden brands, in: Proceedings of the Third International Conference on Fire Research and Engineering, Boston, USA, 1998.

[18] J.P. Woycheese, P.J. Pagni, D. Liepman, Brand propagation from large-scale fires, J. Fire Protect. Eng. 10 (1999) 32–44.

[19] J.P. Woycheese, Wooden disk combustion for spot fire spread, in: Proceedings of the Ninth Interflam, Edinburgh, 2001.

[20] S.D. Tse, A.C. Fernandez-Pello, On the flight paths of metal particles and embers generated by power lines in high winds—a potential source of wildland fires, Fire Saf. J. 30 (1998) 333–356.

[21] R.A. Anthenien, S.D. Tse, A.C. Fernandez-Pello, On the trajectories of embers initially elevated or lofted by small scale ground fire plumes in high winds, Fire Saf. J. 41 (2006) 349–363.

[22] K. Himoto, T. Tanaka, Transport of disk-shaped firebrands in a turbulent boundary layer, in: Proceedings of the Eighth International Symposium on Fire Safety Science, 2005, pp. 433–441.

[23] N. Sardoy, J.L. Consalvi, B. Porterie, A.C. Fernandez-Pello, Modeling transport and combustion of firebrands from burning trees, Combust. Flame 150 (2007) 151–169.

[24] N. Sardoy, J.L. Consalvi, A. Kaiss, A.C. Fernandez-Pello, B. Porterie, Numerical study of ground-level distribution of firebrands generated by line fires, Combust. Flame 154 (2008) 478–488.

[25] C. Lindenburg, Stall coefficients, aerodynamic airfoil coefficients at large angles of attack, in: Proceedings of the IAE symposium on the Aerodynamics of Wind Turbines, ECNRX-01-004, NREL, USA, 2000.

[26] H. Clift, W.H. Gauvin, The motion of particles in turbulent gas stream, in: Proceedings of the Chemeca, vol. 70(1), 1970.

[27] J.D. Holmes, C.W. Letchford, L. Ning, Investigations of plate-type windborne debris—Part II: computed trajectories, J. Wind Eng. Ind. Aerodyn. 94 (2000) 21–39.